ACS NANO

www.acsnano.org

ARTICLE

# Correlation between the Electrical Properties and Formation Temperature of Self-assembled Monolayer-Based Molecular Junctions

Hyemin Lee, Haeri Kim, Donguk Kim, Jongwoo Nam, Minwoo Song, Hyun Sun Sung, Jaegeun Noh,* and Takhee Lee*

Cite This: *ACS Nano* 2025, 19, 36223−36231

Read Online

ACCESS | Metrics & More | Article Recommendations | Supporting Information

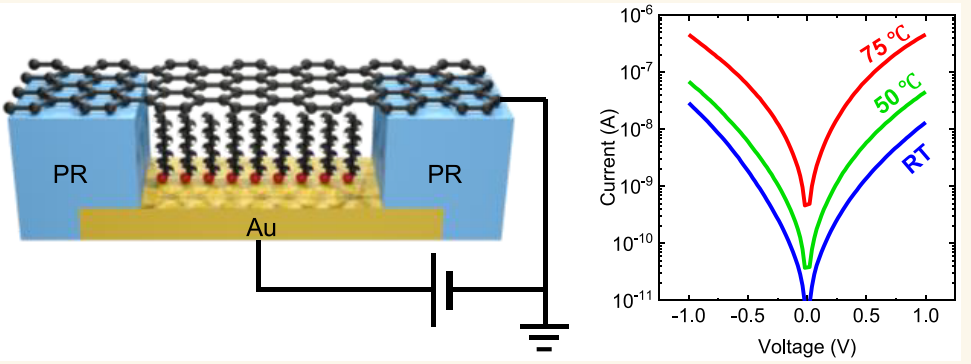


**ABSTRACT:** Self-assembled monolayers (SAMs) of molecules have been reported to exhibit improved structural quality when formed at elevated temperatures; however, this effect has long been ignored in the field of molecular electronics. In this study, electrical measurements such as current−voltage characteristics were combined with scanning tunneling microscopy (STM) images to analyze the correlation between the SAM formation temperature and the resulting electrical properties of SAM junctions using alkanethiol. Increasing the formation temperature enhanced the conductance of the SAM junctions, which is associated with the improved structural quality of the SAMs with fewer defects and larger domains. Additionally, the rectifying behavior was found to be related to the conductance of the SAMs. A close examination of the current−voltage characteristics revealed that rectification was due to an asymmetrical shift of the highest occupied molecular orbital (HOMO) under bias. Defects in SAMs account for rectification, as well as its correlation with conductance. Based on these observations, it was found that the formation temperature affects the electronic properties of the SAM junctions by controlling the defects. This study elucidates the causal relationship between the SAM formation process and the resulting electrical properties of SAM junctions.

**KEYWORDS:** *self-assembled monolayers, electrical properties, molecular electronic junctions, formation temperature, defects*

## INTRODUCTION

Understanding charge transport in self-assembled monolayers (SAMs) is critical for molecular electronics, as SAMs are key building blocks for implementing reliable large-area junctions in a variety of device applications, including diodes,[1,2] transistors,[3−5] and memristors.[6] SAMs can also be applied to flexible devices that exhibit consistent operation under mechanical stress or interesting responses, such as changes in current or mechano-optoelectronic properties.[7−9] In addition, SAMs with electric dipoles are widely used as functional layers for work function engineering in a patternable manner.[10−17] The

Received: May 8, 2025
Revised: September 24, 2025
Accepted: September 24, 2025
Published: October 4, 2025

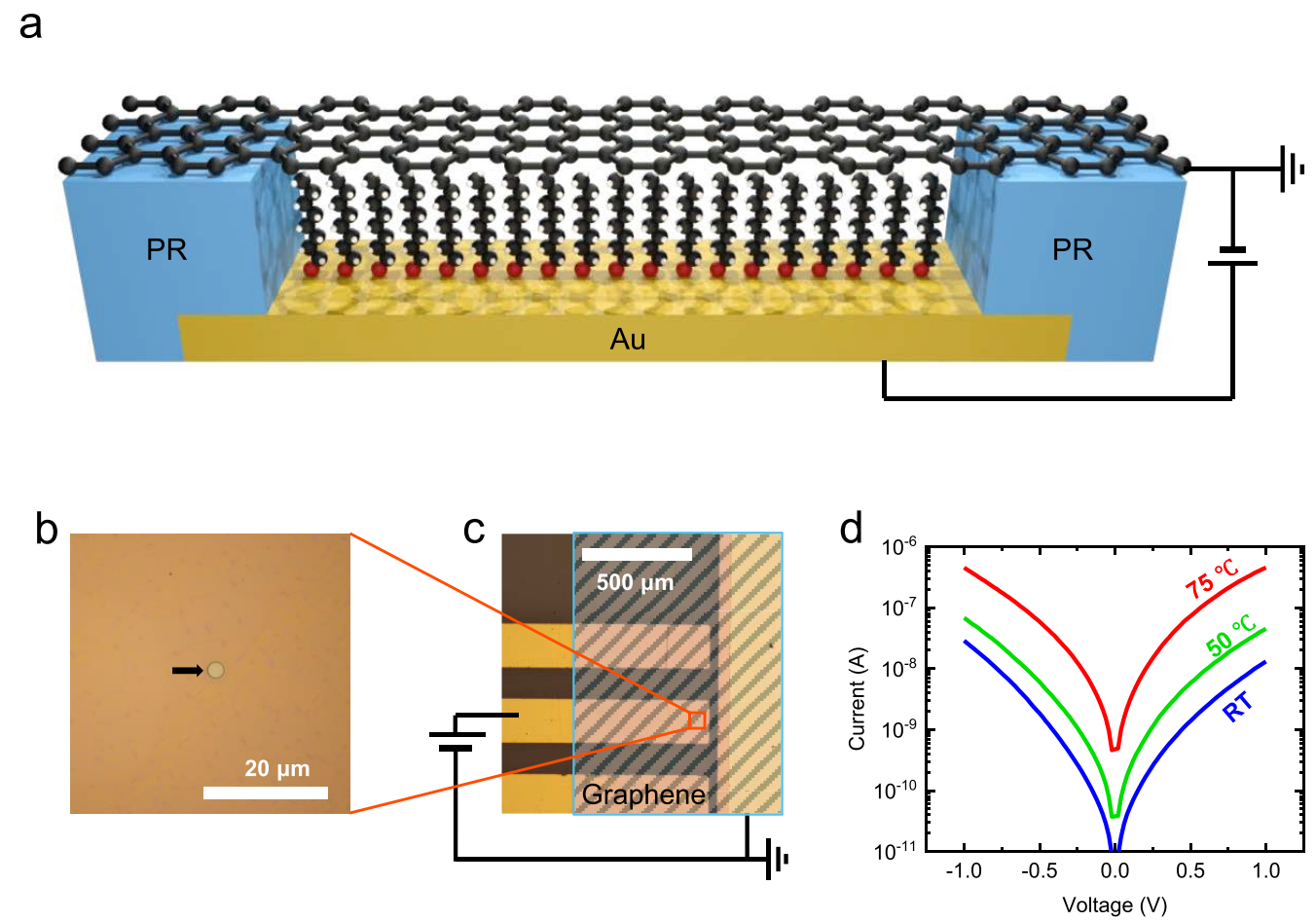


**Figure 1. (a) Schematic illustration of the molecular device. The black, white, and red balls represent carbon, hydrogen, and sulfur atoms, respectively. (b) Optical image of an Au/SAM/graphene junction with PR sidewalls. (c) Zoomed-out image showing 3 molecular junctions. (d) Average current−voltage characteristics of molecular junctions formed at room temperature (blue), 50 °C (green), and 75 °C (red).**

conduction properties through the highest occupied molecular orbital (HOMO) and lowest unoccupied molecular orbital (LUMO) are also useful in charge injection in transistors and photoelectric devices.[15−19]

While SAMs are applied to a wide range of electronics, much effort has been devoted to studying the formation characteristics of SAMs under various conditions, such as temperature, solvent, molecular concentration, and immersion time.[20−28] Detailed adsorption dynamics of thiolated molecules on metal substrates have also been extensively investigated both experimentally and theoretically.[29−34] Since the adsorption process and the quality of SAMs depend on the formation process, it is natural to question the correlation between the formation conditions and the resulting electrical properties of SAMs. In a single-molecule limit, there have been pioneers who elucidated the effect of formation conditions on the electrical properties, but the scope tends to be limited to sharp metal structures.[35] Up to date, efforts to correlate the electrical characteristics to the more intrinsic properties of SAMs have mainly focused on geometric factors, such as tilt angle and conformations.[1,36,37] However, the effects of formation conditions directly controlled at the fabrication level on the electrical properties of SAMs have not been extensively studied.

The formation temperature is known to be a major factor determining the quality of SAMs of both aliphatic and conjugated molecules.[20,21] An elevated formation temperature leads to well-ordered SAMs, reducing the number of vacancy islands and the disordered phases. In this study, we investigated the effect of SAM formation temperature on the electrical properties of octanethiol (C8) SAMs, bridging the knowledge gap between the formation process and the implementation of actual electronic devices. As a primary result, the formation temperature was found to have a positive correlation with the electrical conductance of the SAM junctions. Scanning tunneling microscopy (STM) observations support that the enhancement of conduction is coupled with a decrease in defects and the resulting effective increase in the number of molecular channels. Also, the current rectification characteristics depend on the formation temperature of the SAMs. Linearity was defined as a measure of the linearness of the current−voltage curves and was found to be coupled to rectification. The correlation between linearity and the rectification ratio (RR) suggested that the defects in the SAMs changed the conduction characteristics of the molecular junctions by affecting the HOMO level alignment under bias. This study reveals that the formation process of SAMs can significantly change their conduction characteristics, which is noteworthy when molecular devices are implemented using SAMs as functional elements.

## RESULTS AND DISCUSSION

Figure 1a shows a schematic of the molecular device used in this study. Sandwiching C8 SAM between the Au bottom electrode and the graphene top electrode, the device structure provides a



https://doi.org/10.1021/acsnano.5c07611
ACS Nano 2025, 19, 36223−36231

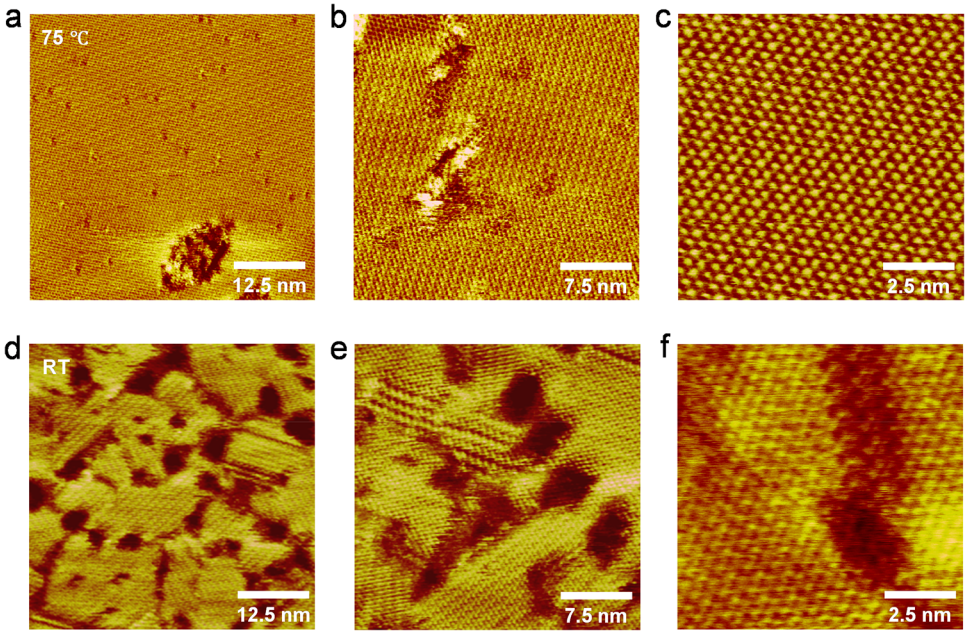


**Figure 2. STM images of C8 SAMs formed at (a–c) 75 °C and (d–f) room temperature.**

testbed for two-terminal current–voltage measurements of vertical SAM junctions. For electrical measurements, the graphene electrode was grounded, and a voltage was applied to the Au electrode. Template-stripped Au provides a flat substrate for large-area SAMs of up to a few microns.[38−41] Photoresist (PR) sidewalls were used as patternable and insulating films to form uniform dimensions of molecular junctions. Figure 1a shows a comprehensive yet not-in-scale illustration, and the junction structure with realistic relative length scales is provided in the Supporting Information (Figure S3). Figure 1b shows an optical image of a circular molecular junction with a radius of 2 $\mu$m (indicated by an arrow in Figure 1b). In Figure 1c, the horizontal Au pads (bottom electrodes) and the top graphene electrode (marked as a dashed area) form of multiple molecular junctions. The detailed fabrication process and characterization of the template-stripped Au and graphene films can be found in the Experimental Section and Supporting Information (Sections 1 and 2). C8 SAMs in the molecular junctions were prepared at three different temperatures: room temperature (RT), 50 °C, and 75 °C. All components of devices, including PR, were found to be compatible with the formation temperature ranging from RT to 75 °C. Despite some apparent damage to the PR after immersion in ethanol at high temperature, the PR wall remained insulating, and the radius of aperture remained unchanged, providing a good platform for a formation-temperature-dependent experiment with a well-defined size of the molecular junction. The results of the compatibility tests can be found in the Supporting Information (Section 3). The formation of uniform octanethiol SAMs on template-stripped Au at temperatures from RT to 75 °C was also confirmed by contact angle measurements (Supporting Information Section 4).

Representative current–voltage characteristics in the log scale are presented in Figure 1d, obtained by averaging the individual data from 166, 116, and 158 working molecular junctions formed at RT, 50 °C, and 75 °C, respectively. All acquired data were classified as working or not by the quantitative criteria presented in the Experimental Section and Supporting Information (Section 5). Notably, the SAMs formed at elevated temperatures showed a larger conductance. For example, the conductance of SAMs formed at 75 °C was about 60-fold larger than that formed at RT near zero voltage, which emphasizes the importance of controlling the formation process of SAMs in the junction fabrication process. The increase of conductance of the molecular junction at a high formation temperature was also observed for decanethiol and dodecanethiol, implying the generality of this effect on alkanethiol SAMs (Supporting Information Section 6).

Template-stripped Au is a good substrate for the fabrication of SAM-based electronic devices due to its relatively uniform surface morphology.[38−41] However, it is very difficult to obtain molecular-scale information about C8 SAMs on the template-stripped Au substrate because it contains many small-sized, flat terraces ranging from a few nanometers to ~40 nm, as shown in the STM images in Supporting Information (Section 7). In this study, single-crystal Au(111) substrates with terraces larger than ~100 nm were used to determine the molecular features of the C8 SAMs (Supporting Information Section 7). The STM images in Figure 2 clearly show that there are significant differences in the molecular features of C8 SAMs on Au(111) depending on the formation temperature. C8 SAMs formed at 75 °C (Figure 2a–c) have long-range, well-ordered domains without domain boundaries. The packing structure of the ordered domains can be assigned to the well-known c(4 × 2) structure observed for various alkanethiolate SAMs.[20,42,43] The density of structural defects, such as vacancy islands and domain boundaries, which are typically observed in alkanethiolate SAMs, was found to be significantly reduced compared with the SAMs formed at RT (Figure 2d–f). STM images (Figure 2d,e) show many small ordered domains separated by domain boundaries and numerous vacancy islands. Magnified STM image (Figure 2f) also shows structural defects in the closely packed ordered domains. STM observations clearly demonstrate that well-ordered SAMs with fewer structural defects can be formed at an elevated formation temperature of 75 °C driven by the Ostwald ripening process.[20,32] Therefore, it is reasonable to consider that highly ordered C8 SAMs can be formed at


https://doi.org/10.1021/acsnano.5c07611
ACS Nano 2025, 19, 36223−36231

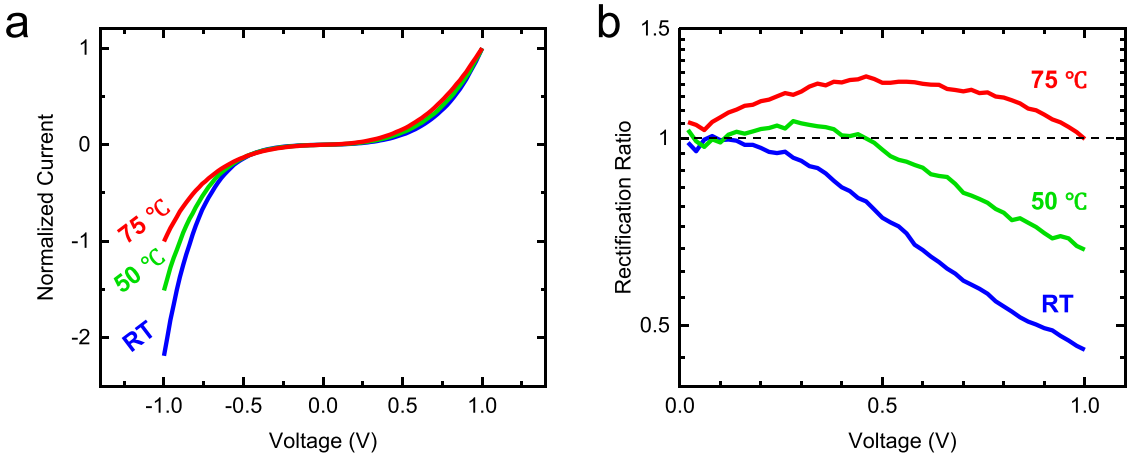


**Figure 3. (a) Current−voltage characteristics of C8 junctions formed at different formation temperatures, normalized by the current at 1.0 V. (b) RR−voltage plot for the averaged current−voltage curves for each formation temperature.**

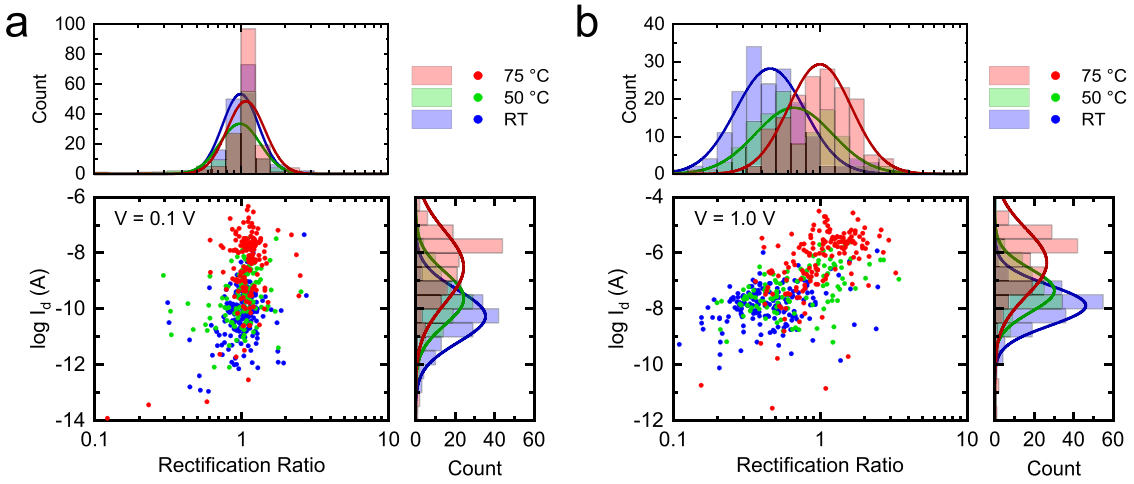


**Figure 4. Scatter plots and histograms for RR and current in the log scale, measured at (a) 0.1 V and (b) 1.0 V. The blue, green, and red symbols correspond to the devices formed at room temperature, 50 °C, and 75 °C, respectively. Gaussian envelopes are also plotted in the histograms for convenience.**

higher formation temperatures also on a template-stripped Au substrate.

When the electrical properties and STM images are combined, the increase in conductance at elevated formation temperatures is attributed to an increase in the number of molecules in close-packed structures. A tunneling model commonly used for C8 molecular junctions predicts the conductance based on three factors: coupling between the molecule and electrodes, HOMO level, and the number of molecular channels.[44] Among them, coupling is unlikely to be changed significantly by formation temperatures, as discussed in Supporting Information (Section 13). Also, the same c(4 × 2) phase is observed for both formation temperatures of RT and 75 °C (Figure 2); thus, it is unlikely that the thickness or tilt angle of the SAMs will change depending on the formation temperature. Especially at zero voltage, the HOMO level is unaffected by the applied voltage, leaving the difference in conductance as the result of the different numbers of channels. Therefore, the observed difference in zero-voltage conductance in Figure 1d can be interpreted as the effect of the formation temperature on the number of conduction channels. We also found that the conductance of molecular junctions is sensitive to the temperature at the beginning of the formation of SAMs, as shown in Supporting Information (Section 8). The full coverage of SAM is reached in a short time scale compared to the immersion time of 20 h (see the Experimental Section).[24,28] Hence, the strong dependence of conductance on the initial temperature implies that the conductance is mainly affected by the temperature during the adsorption process of the SAMs.

Figure 3a shows the average current−voltage data for the molecular junctions (a total of 446 junctions) normalized by the current at 1.0 V. The molecular junctions of SAMs formed at RT exhibited more asymmetric conduction behavior than those formed at 75 °C. As a measure of asymmetry, the rectification ratio (RR) was defined as $RR(V) = I(V)/I(-V)$, where $V$ is a positive voltage and $I$ is the current. An RR = 1 corresponds to the symmetric case, and RR < 1 represents a rectifying junction favorable to negative voltage. Figure 3b shows the averaged RR values (from 446 junctions) plotted as a function of voltage for each formation temperature. The RR of molecular junctions formed at RT decreases (deviating from 1, becoming more asymmetric) as the applied voltage increases, while the RR of those formed at 75 °C remains almost symmetric (i.e., remains at around RR ∼ 1). Rectifying properties decrease smoothly from RT to 75 °C through 50 °C without abrupt changes, which


https://doi.org/10.1021/acsnano.5c07611
ACS Nano 2025, 19, 36223−36231

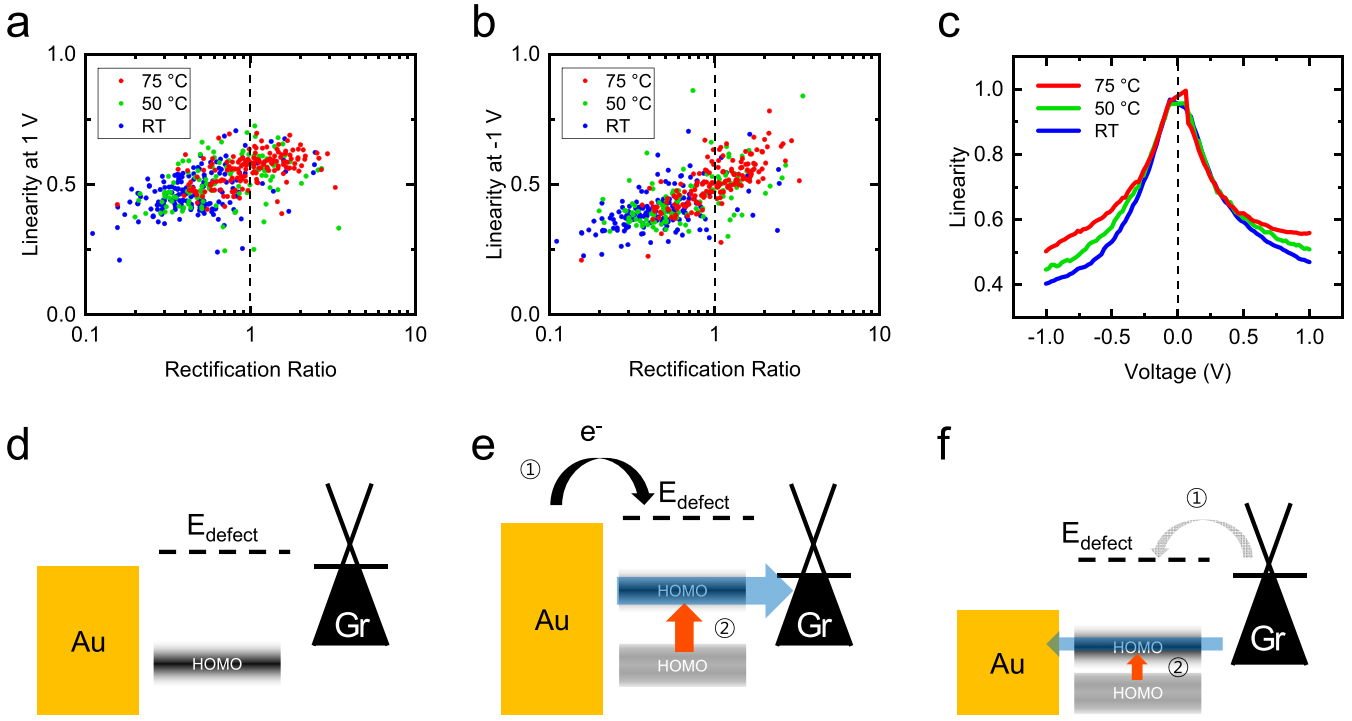


**Figure 5. Scatter plots of the RR and linearity at (a) 1.0 V and (b) −1.0 V. (c) Linearity of the averaged currents of each formation temperature plotted as a function of voltage. (d) Energy band diagram across the molecular junction at zero voltage. Defect states are indicated by a single dashed line, and graphene is abbreviated as Gr for convenience. (e) Energy band diagram under negative voltage, resulting in the charging of defect states and consequent upward shift of the HOMO. (f) Energy band diagram under positive voltage, showing weak charging of defect states due to the lack of density of states in graphene, and thus, a weak upward shift of the HOMO.**

shows a similar trend with the gradual change in the quality of SAMs under varying formation temperatures.[20]

It is notable that the deviation in RR is observed in a relatively high-voltage regime (~1.0 V), whereas the three curves in Figure 3b meet in the low-voltage regime. A common approach to explain rectification is to introduce asymmetry in the HOMO shift under the application of voltage.[2,45−47] For quantitative analysis, the asymmetry factor $\eta$ is used to describe the HOMO shift under bias, or equivalently, the asymmetric voltage drop between the molecule and two electrodes by $\eta$V and $(1-\eta)$V, respectively.[48−50] The asymmetric structure of the Au/SAM/graphene junction may induce rectifying behavior described by $\eta$, which is the result of an asymmetric voltage drop at the Au−S bond and methyl/graphene interface. However, the effect of the asymmetric structure is weak for alkanethiols, where the HOMO lies deep relative to the Fermi level. Moreover, the nature of the electrode-molecule does not change with the formation temperature (Supporting Information Section 13). Thus, the difference in the RR for the three formation temperatures in Figure 3b cannot be attributed to the asymmetric contact itself. More detailed discussions on the rectification and structural asymmetry are provided in the Supporting Information (Section 10).

A combined, closer inspection of the current level and RR reveals a clear correlation with the formation temperature, as shown in Figure 4a,b. As shown in Figure 4a, at a voltage as low as 0.1 V, the three formation temperatures deviate in the current level (right panel), while there is no significant difference in the RR (top panel). The scatter plot in Figure 4a does not show any significant correlation between the current and rectification at 0.1 V. On the other hand, at high voltages, such as 1.0 V plotted in Figure 4b, the peaks of the RR values for each formation temperature are separated (top panel), while the current scale has the same positive correlation to formation temperatures as at 0.1 V (right panel). This immediately results in a correlation between the current level and RR; that is, a junction with higher conductance shows more symmetric current−voltage characteristics (scatter plot in Figure 4b). It is worth noting that the separated scatter plots for each formation temperature show the same trend, that is, higher conductance is correlated with more symmetric behavior (Figure S23, Supporting Information). That is, the conductance is correlated to rectification, rather than the formation temperature itself. The same trend is observed for negative voltages, as shown in Figure S24 in the Supporting Information.

It is convenient to define a quantity "linearity" (denoted by $L$), which is a measure of linearness of the current−voltage curve, defined as

$$L(V) = \frac{\int_0^V \mathrm{d}V' I(V')}{\frac{I(V)\cdot V}{2}} \quad (1)$$

The basic properties of $L$ are discussed in the Supporting Information (Section 12). The linearity $L$ in a high-voltage regime shows a clear correlation with RR, as shown in Figure 5a,b for ±1.0 V. Though the current at ±1.0 V also showed a correlation with RR (Figures 4b and S24), RR was coupled to L stronger than the current. Especially, at −1.0 V, the correlation between RR and linearity was as high as 0.70, while that between RR and current remained at 0.41. This implies that the rectifying properties of the junctions are affected by linearity more directly than by the current level. Figure 5c presents the $L(V)$ characteristics for each formation temperature. All three curves in Figure 5c coincide in the low-voltage regime. As the applied



https://doi.org/10.1021/acsnano.5c07611
ACS Nano 2025, 19, 36223−36231

voltage increases, the linearities decay and deviate from each other. The linearity of the junctions formed at higher temperatures is larger than that of the junctions formed at lower temperatures at high voltages, indicating that the molecular junctions formed at elevated temperatures result in more linear current−voltage curves.

The current in the molecular junction is determined by the voltage, coupling between molecules and electrodes, number of molecules, and HOMO level.[44] Because linearity is a normalized quantity, the number of molecules does not affect it. Also, the coupling constants do not alter $L(V)$ characteristics significantly, even under a 100-fold change in the coupling constants (Supporting Information Section 12). Noting that the formation temperature does not affect the nature of the molecule−electrode coupling, therefore, the differences in the $L(V)$ characteristics for different formation temperatures are not likely to originate from the coupling. Thus, at a given voltage, $L(V)$ is mainly affected by the HOMO level. Simulations based on the Landauer formalism (Figure S28) show that linearity is enhanced when the HOMO level is deep or, equivalently, far from the Fermi level (Supporting Information Section 12). For all three formation temperatures, the linearity is slightly larger at positive voltage than at negative voltage (Figure 5c), which can be attributed to the asymmetric voltage drop at the molecule−electrode interfaces induced by the asymmetric structure of the SAM junction investigated in this study (Supporting Information Section 12). Figure 5c shows that the HOMO level of SAMs formed at elevated temperatures tends to remain deeper, while that of SAMs formed at lower temperatures becomes shallower in the high-voltage regime. Note that the linearity $L$ of the molecular junctions also shows a positive correlation with the zero-voltage conductance which is proportional to the number of molecules in the junction (see Supporting Information Section 15).

Figure 5d depicts the energy band diagram describing the HOMO level shift affected by the defects. Defect states lying on imperfections in SAMs are illustrated with the HOMO and electrodes. It should be noted that the defect states are marked as a single line for simplicity, while they may be distributed over a broad range of energies. A slight p-doping of graphene induced by the wet-transfer process and Fermi level matching to Au/SAM is also illustrated.[51,52] For detailed characterization of the energy structure of the SAM junction, including the HOMO level (about −2.4 eV below the Fermi level) and doping level of graphene, see Supporting Information (Sections 16 and 17). When a negative voltage is applied to the junction, the defect states are filled by the Au electrode which behaves as an electron reservoir, and negatively charged defects lead to an upshift of the HOMO to a shallower energy state, as shown in Figure 5e. Hence, the defects result in an increase in the current at negative voltages, accounting for the RR and lower linearity at negative biases. This effect is prominent for SAMs formed at RT which have more imperfections. On the other hand, positive voltage results in weak charge filling from graphene which suffers from a lack of DOS and consequent quantum capacitance[53,54] that leads to a less p-doped configuration under positive voltage, as depicted in Figure 5f. This weakens the upward shift of the HOMO, leaving the linearity higher than that at negative voltages, as discussed above.

Here, the differences in the transport characteristics are mainly due to the changes in the SAMs rather than the graphene electrode. For example, ultraviolet (UV) photoelectron spectroscopy (UPS) and Raman spectroscopy revealed that the work function or carrier density of graphene on SAMs formed at RT and 75 °C did not show significant differences (Supporting Information Section 17). Moreover, because the SAMs are the main source of electric resistance in the Au/SAM/graphene structure, small changes in the electric properties of graphene on the SAMs can be neglected.

From the zero-voltage conductance (Supporting Information Section 15) and STM image (Figure 2), SAM junctions formed at elevated temperatures are expected to have a low number of defect states, which implies a lesser effect on the HOMO shifting under voltage depicted in Figure 5d−f. Hence, with a lower source of asymmetry, the junctions formed at 75 °C showed an RR near unity and more linear current−voltage characteristics. On the other hand, lower formation temperatures lead to more upward shifts of the HOMO due to more defects, especially at negative voltages, hence giving a rectifying and less linear current response.

## CONCLUSIONS

In summary, this study demonstrated that the formation temperature of SAMs affects the conduction properties of SAM junctions. Electrical measurements showed that the conductance increased 60 times compared to that of the SAMs formed at room temperature when the SAM formation temperature increased to 75 °C. The variation in the conductance is attributed to the difference in the number of close-packed molecular channels, which is also supported by the STM images. In addition, SAM junctions formed at different temperatures showed different rectifying properties, i.e., more symmetric current−voltage characteristics when formed at higher temperatures. Statistical analysis showed a correlation between the current order and rectification in the high-voltage regime, which is due to the HOMO level shift under bias. We presented a model explaining the HOMO level shift due to the defect states in SAMs. A high formation temperature led to a decrease in defects and a weakening of the defect-induced HOMO shift. The rectifying or symmetric and linear or nonlinear conduction characteristics of the SAMs were found to be related to the formation temperature, which was explained by the proposed model. Therefore, this study provides a basis for understanding the relationship between the formation process of SAMs and the resulting electrical properties.

## EXPERIMENTAL SECTION

**Device Fabrication and Electrical Measurements.** All devices were fabricated on a template-stripped Au substrate, with an atomically smooth surface.[38−41] To prepare this substrate, a 50 nm-thick Au film was deposited on a clean silicon surface by e-beam evaporation. The Au film was patterned as electrodes using shadow masks during evaporation. After optical adhesive (OA) (NOA61, Norland) was cast on the Au/silicon substrate, the substrate was covered with glass that had been treated with ultraviolet (UV) light for Au adhesion. UV curing for an hour and overnight aging in a 50 °C oven under low vacuum were performed to obtain a chemically stable OA mold for Au. Finally, a razor was used to eliminate the silicon substrate to expose the ultraflat Au surface, giving an Au/OA/glass substrate for forming molecular junctions. On this substrate, the PR sidewall was patterned using photolithography, resulting in multiple pairs of Au electrodes and holes with a radius of 2 $\mu$m in the PR layer on the electrodes. PR was hard baked at 200 °C for 30 min under a constant argon flow with 5% hydrogen to prevent the oxidation of Au surfaces. Then, patterned substrates were immersed in a 5 mM ethanol solution of C8 at the designated formation temperature in a glovebox filled with nitrogen (both ethanol and C8 were purchased from Sigma-Aldrich). For accurate temperature control, all the solutions and substrates were


https://doi.org/10.1021/acsnano.5c07611
ACS Nano 2025, 19, 36223−36231

heated to the desired temperature before immersion. The immersion time was at least 20 h and not more than 24 h. After the formation of SAMs, the substrates were rinsed with ethanol, and then the graphene film was transferred onto the SAMs/Au/OA/glass structure by wet transfer.

A chemical vapor deposition-grown graphene film (purchased from Graphene Square) was initially prepared in the form of poly(methyl methacrylate) (PMMA)/graphene/copper foil for the top electrode. A 0.2 M aqueous solution of ammonium persulfate was used for etching the copper foil, and the remaining PMMA/graphene was cleaned by floating it three times on deionized water for more than 10 min to eliminate physisorbed ions and contaminants. After the wet transfer of graphene, PMMA was etched by immersing the devices in acetone for 5 min, and graphene was etched using oxygen plasma with a shadow mask to obtain the desired pattern. More detailed fabrication processes are provided in Supporting Information (Section 1). The characterization results of the Au roughness and graphene are presented in Supporting Information (Section 2).

Electrical measurements were performed in a vacuum probe station. The voltage was swept from 0 to 1 V to avoid breakdown caused by abrupt bias stress, and then data was acquired with decreasing voltage to −1.0 V with a step of −0.02 V. Then, the voltage was set to 0 V before disconnecting the molecular junction. All junctions were classified into one of four categories: open, noisy, short, or working. Open was clearly distinguished with its extremely low current level on the sub-pA scale, with almost no response to voltage. For example, junctions showing a sub-pA current at ±1 V were classified as open. Noisy cases showed large hysteresis or noise, hindering an accurate analysis. Since they tend to show sharp peaks in the current−voltage curves, junctions that showed such unusual behaviors were classified as noisy, with a quantitative criterion provided in Supporting Information (Section 5). After excluding open and noisy cases, junctions with $G(1.0\ \mathrm{V})/G(0.1\ \mathrm{V}) < 5$ were classified as short, where $G(V) = I(V)/V$, as they are much more linear than that expected in Au/C8/graphene junctions. The others were all classified as working. Typical current−voltage characteristics for all four cases are presented in the Supporting Information (Section 5).

**STM Imaging.** C8 SAMs for STM imaging were prepared on single-crystal Au(111) substrates with large, atomically flat terraces by the thermal evaporation of Au onto a freshly cleaved mica surface preheated to 570 K under ultrahigh vacuum conditions of approximately $10^{-5}$ Pa. C8 SAMs were prepared by immersing Au(111) substrates in a 5 mM ethanol solution containing C8 molecules at RT and 75 °C for 24 h. After SAM formation, the substrates were taken out of the solution and immediately rinsed with pure ethanol to remove the physisorbed molecules on the surface. STM measurements were performed in constant current mode in air using a NanoScope E (Veeco, Santa Barbara, CA) with a commercially available Pt/Ir (80:20) tip.

## ASSOCIATED CONTENT

### Supporting Information

The Supporting Information is available free of charge at https://pubs.acs.org/doi/10.1021/acsnano.5c07611.

Additional details on the fabrication process, characterization of electrodes and PR sidewalls; additional plots and data on electrical measurements on SAMs formed at nonconstant temperatures; simulations on rectification and linearity of current−voltage characteristics; and detailed discussions on the linearity, zero-voltage conductance, and their correlations (PDF)

## AUTHOR INFORMATION


### Corresponding Authors

**Jaegeun Noh** − *Department of Chemistry and Research Institute for Convergence of Basic Science, Hanyang University, Seoul 04763, Korea;* orcid.org/0000-0002-6115-7971; Email: jgnoh@hanyang.ac.kr

**Takhee Lee** − *Department of Physics and Astronomy, and Institute of Applied Physics, Seoul National University, Seoul 08826, Korea;* orcid.org/0000-0001-5988-5219; Email: tlee@snu.ac.kr

### Authors

**Hyemin Lee** − *Department of Physics and Astronomy, and Institute of Applied Physics, Seoul National University, Seoul 08826, Korea;* orcid.org/0009-0001-5285-4484

**Haeri Kim** − *Department of Chemistry and Research Institute for Convergence of Basic Science, Hanyang University, Seoul 04763, Korea*

**Donguk Kim** − *Department of Physics and Astronomy, and Institute of Applied Physics, Seoul National University, Seoul 08826, Korea*

**Jongwoo Nam** − *Department of Physics and Astronomy, and Institute of Applied Physics, Seoul National University, Seoul 08826, Korea*

**Minwoo Song** − *Department of Physics and Astronomy, and Institute of Applied Physics, Seoul National University, Seoul 08826, Korea*

**Hyun Sun Sung** − *Department of Chemistry and Research Institute for Convergence of Basic Science, Hanyang University, Seoul 04763, Korea*

Complete contact information is available at: https://pubs.acs.org/10.1021/acsnano.5c07611


### Notes

The authors declare no competing financial interest.

## ACKNOWLEDGMENTS

The authors appreciate the financial support of the National Research Foundation of Korea (NRF) grant (No. 2021R1A2C3004783 and No. RS-2023-00220471) and the Nano Material Technology Development Program grant (No. 2021M3H4A1A02049651) through the NRF funded by the Ministry of Science and ICT (MSIT) of Korea. H.K., H.S.S., and J.Noh. acknowledge the NRF grant (No. 2020R1A6A1A06046728) from MSIT of Korea.

## REFERENCES

(1) Eo, J. S.; Shin, J.; Jeon, T.; Jang, J.; Wang, G. Tilt-Engineered Molecular-Scale Selector for Enhanced Learning in Artificial Neural Networks. *Adv. Funct. Mater.* **2024**, *34*, No. 2311103.

(2) Nijhuis, C. A.; Reus, W. F.; Barber, J. R.; Dickey, M. D.; Whitesides, G. M. Charge Transport and Rectification in Arrays of SAM-Based Tunneling Junctions. *Nano Lett.* **2010**, *10*, 3611−3619.

(3) Sasao, K.; Azuma, Y.; Kaneda, N.; Hase, E.; Miyamoto, Y.; Majima, Y. Observation of Current Modulation through Self-Assembled Monolayer Molecule in Transistor Structure. *Jpn. J. Appl. Phys.* **2004**, *43*, L337−L339.

(4) Famili, M.; Jia, C.; Liu, X.; Wang, P.; Grace, I. M.; Guo, J.; Liu, Y.; Feng, Z.; Wang, Y.; Zhao, Z.; Decurtins, S.; Häner, R.; Huang, Y.; Liu, S.-X.; Lambert, C. J.; Duan, X. Self-Assembled Molecular-Electronic Films Controlled by Room Temperature Quantum Interference. *Chem* **2019**, *5*, 474−484.

(5) Wang, X.; Ismael, A.; Ning, S.; Althobaiti, H.; Al-Jobory, A.; Girovsky, J.; Astier, H. P. A. G.; O'Driscoll, L. J.; Bryce, M. R.; Lambert, C. J.; Ford, C. J. B. Electrostatic Fermi Level Tuning in Large-Scale Self-Assembled Monolayers of Oligo(phenyleneethynylene) Derivatives. *Nanoscale Horiz.* **2022**, *7*, 1201−1209.

(6) Wang, Y.; Zhang, Q.; Astier, H. P. A. G.; Nickle, C.; Soni, S.; Alami, F. A.; Borrini, A.; Zhang, Z.; Honnigfort, C.; Braunschweig, B.; Leoncini, A.; Qi, D.-C.; Han, Y.; del Barco, E.; Thompson, D.; Nijhuis, C. A. Dynamic Molecular Switches with Hysteretic Negative Differ-

ential Conductance Emulating Synaptic Behaviour. *Nat. Mater.* **2022**, *21*, 1403−1411.
(7) Yang, Z.; Cazade, P.-A.; Lin, J.-L.; Cao, Z.; Chen, N.; Zhang, D.; Lian, D.; Nijhuis, C. A.; Thompson, D.; Li, Y. High Performance Mechano-Optoelectronic Molecular Switch. *Nat. Commun.* **2023**, *14*, No. 5639.
(8) Park, S.; Wang, G.; Cho, B.; Kim, Y.; Song, S.; Ji, Y.; Yoon, M.-H.; Lee, T. Flexible Molecular-Scale Electronic Devices. *Nat. Nanotechnol.* **2012**, *7*, 438−442.
(9) Wang, G.; Kim, T.-W.; Jo, G.; Lee, T. Enhancement of Field Emission Transport by Molecular Tilt Configuration in Metal-Molecule-Metal Junctions. *J. Am. Chem. Soc.* **2009**, *131*, 5980−5985.
(10) Zhang, C.; Liu, Y.; Tai, Y.; Terfort, A.; Zharnikov, M. Location-Selective Work Function Engineering by Self-Assembled Monolayers. *J. Phys. Chem. Lett.* **2024**, *15*, 4581−4586.
(11) Liu, D.; Mia, Q. Recent Progress in Interface Engineering of Organic Thin Film Transistors with Self-Assembled Monolayers. *Mater. Chem. Front.* **2018**, *2*, 11−21.
(12) Yan, Z.; Sun, Z.; Lu, W.; Yao, J.; Zhu, Y.; Tour, J. M. Controlled Modulation of Electronic Properties of Graphene by Self-Assembled Monolayers on $SiO_2$ Substrates. *ACS Nano* **2011**, *5*, 1535−1540.
(13) Kim, S. Y.; Cho, S. J.; Byeon, S. E.; He, X.; Yoon, H. J. Self-Assembled Monolayers as Interface Engineering Nanomaterials in Perovskite Solar Cells. *Adv. Energy Mater.* **2020**, *10*, No. 2002606.
(14) Yalcin, E.; Can, M.; Rodriguez-Seco, C.; Aktas, E.; Pudi, R.; Cambarau, W.; Demic, S.; Palomares, E. Semiconductor Self-Assembled Monlayers as Selective Contacts for Efficient PiN Perovskite Solar Cells. *Energy Envrion. Sci.* **2019**, *12*, 230−237.
(15) Borchert, J. W.; Peng, B.; Letzkus, F.; Burghartz, J. N.; Chan, P. K. L.; Zojer, K.; Ludwigs, S.; Klauk, H. Small Contact Resistance and High-Frequency Operation of Flexible Low-Voltage Inverted Coplanar Organic Transistors. *Nat. Commun.* **2019**, *10*, No. 1119.
(16) Chen, H.; Zhang, W.; Li, M.; He, G.; Guo, X. Interface Engineering in Organic Field-Effect Transistors: Principles, Applications, and Perspectives. *Chem. Rev.* **2020**, *120*, 2879−2949.
(17) Choi, K.; Choi, H.; Min, J.; Kim, T.; Kim, D.; Son, S. Y.; Kim, G.-W.; Choi, J.; Park, T. A Short Review on Interface Engineering of Perovskit Solar Cells: A Self-Assembled Monolayer and Its Roles. *Sol. RRL* **2020**, *4*, No. 1900251.
(18) Mei, Y.; Fogel, D.; Chen, J.; Ward, J. W.; Payne, M. M.; Anthony, J. E.; Jurchescu, O. D. Interface Engineering to Enhance Charge Injection and Transport in Solution-Deposited Organic Transistors. *Org. Electron.* **2017**, *50*, 100−105.
(19) Singh, K. A.; Nelson, T. L.; Belot, J. A.; Young, T. M.; Dhumal, N. R.; Kowalewski, T.; McCullough, R. D.; Nachimuthu, P.; Thevuthasan, S.; Porter, L. M. Effect of Self-Assembled Monolayers on Charge Injection and Transport in Poly(3-hexylthiophene)-Based Field-Effect Transistors at Different Channel Length Scales. *ACS Appl. Mater. Interfaces* **2011**, *3*, 2973−2978.
(20) Yamada, R.; Wano, H.; Uosaki, K. Effect of Temperature on Structure of the Self-Assembled Monolayer of Decanethiol on Au(111) Surface. *Langmuir* **2000**, *16*, 5523−5525.
(21) Kang, H.; Park, T.; Choi, I.; Lee, Y.; Ito, E.; Hara, M.; Noh, J. Formation of Large Ordered Domains in Benzenethiol Self-Assembled Monolayers on Au(111) Observed by Scanning Tunneling Microscopy. *Ultramicroscopy* **2009**, *109*, 1011−1014.
(22) Castner, D. G.; Hinds, K.; Grainger, D. W. X-ray Photoelectron Spectroscopy Sulfur 2p Study of Organic Thiol and Disulfide Binding Interactions with Gold Surfaces. *Langmuir* **1996**, *12*, 5083−5086.
(23) Käfer, D.; Witte, G.; Cyganik, P.; Terfort, A.; Wöll, C. A Comprehensive Study of Self-Assembled Monolayers of Anthracenethiol on Gold: Solvent Effects, Structure, and Stability. *J. Am. Chem. Soc.* **2006**, *128*, 1723−1732.
(24) Bain, C. D.; Troughton, E. B.; Tao, Y.-T.; Evall, J.; Whitesides, G. M.; Nuzzo, R. G. Formation of Monolayer Films by the Spontaneous Assembly of Organic Thiols from Solution onto Gold. *J. Am. Chem. Soc.* **1989**, *111*, 321−335.
(25) Love, J. C.; Estroff, L. A.; Kriebel, J. K.; Nuzzo, R. G.; Whitesides, G. M. Self-Assembled Monolayers of Thiolates on Metals as a Form of Nanotechnology. *Chem. Rev.* **2005**, *105*, 1103−1170.
(26) Ulman, A. Formation and Structure of Self-Assembled Monolayers. *Chem. Rev.* **1996**, *96*, 1533−1554.
(27) Schwartz, D. K. Mechanisms and Kinetics of Self-Assembled Monolayer Formation. *Annu. Rev. Phys. Chem.* **2001**, *52*, 107−137.
(28) Ogawa, H. O. H.; Takamura, T.; Shimoyama, Y. Self-Assembly Process of Alkanethiol Monolayers. *Jpn. J. Appl. Phys.* **1999**, *38*, 6019−6023.
(29) McCarley, R. L.; Dunaway, D. J.; Willicut, R. J. Mobility of the Alkanethiol-Gold(111) Interface Studied by Scanning Probe Microscopy. *Langmuir* **1993**, *9*, 2775−2777.
(30) Cossaro, A.; Mazzarello, R.; Rousseau, R.; Casalis, L.; Verdini, A.; Kohlmeyer, A.; Floreano, L.; Scandolo, S.; Morgante, A.; Klein, M. L.; Scloes, G. X-ray Diffraction and Computation Yield the Structure of Alkanethiols on Gold(111). *Science* **2008**, *321*, 943−946.
(31) Mazzarello, R.; Cossaro, A.; Verdini, A.; Rousseau, R.; Casalis, L.; Danisman, M. F.; Floreano, L.; Scandolo, S.; Morganter, A.; Scoles, G. Structure of a $CH_3S$ Monolayer on Au(111) Solved by the Interplay between Molecular Dynamics Calculations and Diffraction Measurements. *Phys. Rev. Lett.* **2007**, *98*, No. 016102.
(32) Lee, N.-S.; Kang, H.; Seong, S.; Noh, J. Effect of Immersion Time on the Structure of Octanethiol Self-Assembled Monolayers on Au(111) at an Elevated Solution Temperature. *Bull. Korean Chem. Soc.* **2019**, *40*, 1152−1153.
(33) Barrena, E.; Ocal, C.; Salmeron, M. Structure and Stability of Tilted-Chain Phases of Alkanethiols on Au(111). *J. Chem. Phys.* **2001**, *114*, 4210−4214.
(34) Kautz, N. A.; Kandel, S. A. Alkanethiol/Au(111) Self-Assembled Monolayers Contain Gold Adatoms: Scanning Tunneling Microscopy before and after Reaction with Atomic Hydrogen. *J. Am. Chem. Soc.* **2008**, *130*, 6908−6909.
(35) Dalmieda, J.; Shi, W.; Li, L.; Venkataraman, L. Solvent-Mediated Modulation of the Au-S Bond in Dithiol Molecular Junctions. *Nano Lett.* **2024**, *24*, 703−707.
(36) Frederiksen, T.; Munuera, C.; Ocal, C.; Brandyge, M.; Paulsson, M.; Sanchez-Portal, D.; Arnau, A. Exploring the Tilt-Angle Dependence of Electron Tunneling across Molecular Junctions of Self-Assembled Alkanethiols. *ACS Nano* **2009**, *3*, 2073−2080.
(37) Belding, L.; Root, S. E.; Li, Y.; Park, J.; Baghbanzadeh, M.; Rojas, E.; Pieters, P. F.; Yoon, H. J.; Whitesides, G. M. Conformation, and Charge Tunneling through Molecules in SAMs. *J. Am. Chem. Soc.* **2021**, *143*, 3481−3493.
(38) Hegner, M.; Wagner, P.; Semenza, G. Ultralarge Atomically Flat Template-Stripped Au Surfaces for Scanning Probe Microscopy. *Surf. Sci.* **1993**, *291*, 39−46.
(39) Wagner, P.; Hegner, M.; Güntherodt, H.-J.; Semenza, G. Formation and in Situ Modification of Monolayers Chemisorbed on Ultraflat Template-Stripped Gold Surfaces. *Langmuir* **1995**, *11*, 3867−3875.
(40) Lee, S.; Bae, S.-S.; Medeiros-Ribeiro, G.; Blackstock, J. J.; Kim, S.; Stewart, D. R.; Ragan, R. Scanning Tuneling Microscopy of Template-Stripped Au Surfaces and Highly Ordred Self-Assembled Monolayers. *Langmuir* **2008**, *24*, 5984−5987.
(41) Samorí, P.; Diebel, J.; Löwe, H.; Rabe, J. P. Template-Stripped Gold Supported on Ni as a Substrate for SAMs. *Langmuir* **1999**, *15*, 2592−2594.
(42) Poirier, G. E.; Tarlov, M. J. The c(4 × 2) Superlattice of n-Alkanethiol Monolayers Self-Assembled on Au(111). *Langmuir* **1994**, *10*, 2853−2856.
(43) Camillone, N., III; Chidsey, C. E. D.; Liu, G.-Y.; Scoles, G. Superlattice Structure at the Surface of a Monolayer of Octanethiol Self-Assembled on Au(111). *J. Chem. Phys.* **1993**, *98*, 3503−3511.
(44) Datta, S. Electrical Resistance: an Atomic View. *Nanotechnology* **2004**, *15*, S433−451.
(45) Kang, H.; Kong, G. D.; Byeon, S. E.; Yang, S.; Kime, J. W.; Yoon, H. J. Interplay of Fermi Level Pinning, Marcus Inverted Transport, and


https://doi.org/10.1021/acsnano.5c07611
*ACS Nano* 2025, 19, 36223−36231

Orbital Gating in Molecular Tunneling Junctions. *J. Phys. Chem. Lett.* **2020**, *11*, 8597−8603.
(46) Migliore, A.; Nitzan, A. Nonlinear Charge Transport in Redox Molecular Junctions: A Marcus Perspective. *ACS Nano* **2011**, *5*, 6669−6685.
(47) Jeong, H.; Kim, D.; Wang, G.; Park, S.; Lee, H.; Cho, K.; Hwang, W.-T.; Yoon, M.-H.; Jang, Y. H.; Song, H.; Xing, D.; Lee, T. Redox-Induced Asymmetric Electrical Characteristics of Ferrocene-Alkanethiolate Molecular Devices on Rigid and Flexible Substrates. *Adv. Funct. Mater.* **2014**, *24*, 2472−2480.
(48) Wang, G.; Kim, Y.; Na, S.-I.; Kahng, Y. H.; Ku, J.; Park, S.; Jang, Y. H.; Kim, D.-Y.; Lee, T. Investigation of the Transition Voltage Spectra of Molecular Junctions Considrering Frontier Molecular Orbitals and the Asymmetric Coupling Effect. *J. Phys. Chem. C* **2011**, *115*, 17979−17985.
(49) Kaur, R. P.; Sawhney, R. S.; Engles, D. Effect of Asymmetric Molecule-Electrode Coupling and Molecular Bias on Rectification in Molecular Junctinos. *Appl. Phys. A* **2016**, *122*, No. 1029.
(50) Datta, S.; Tian, W.; Hong, S.; Reifenberger, R.; Henderson, J. I.; Kubiak, C. P. Current-Voltage Characteristics of Self-Assembled Monolayers by Scanning Tunneling Microscopy. *Phys. Rev. Lett.* **1997**, *79*, 2530−2533.
(51) Wang, X.; Ning, S.; Lin, L.; Li, X.; Ford, C. J. B. Tailoring Quantum Transport Efficiency in Molecular Junctions via Doping of Graphene Electrodes. *J. Mater. Chem. C* **2024**, *12*, 5157−5165.
(52) Koo, E.; Ju, S.-Y. Role of Residual Polymer on Chemical Vapor Grown Graphene by Raman Spectroscopy. *Carbon* **2015**, *86*, 318−324.
(53) Büttiker, M.; Thomas, H.; Prêtre, A. Mesoscopic Capacitors. *Phys. Lett. A* **1993**, *180*, 364−369.
(54) Kim, T. H.; Lee, J.; Lee, R.-G.; Kim, Y.-H. Gate-versus Defect-Induced Voltage Drop and Negative Differential Resistance in Vertical Graphene Heterostructures. *npj Comput. Mater.* **2022**, *8*, 50.





https://doi.org/10.1021/acsnano.5c07611
*ACS Nano* 2025, 19, 36223−36231